

## Article

# Hybrid Approach for Multiscale and Multimodal Time-Resolved Diagnosis of Ultrafast Processes in Materials via Tailored Synchronization of Laser and X-ray Sources at MHz Repetition Rates

Nikita Marchenkov<sup>1,2</sup>, Evgenii Mareev<sup>1,3,\*</sup> , Anton Kulikov<sup>1,2</sup> , Fedor Pilyak<sup>1,2</sup>, Eduard Ibragimov<sup>1,2</sup>, Yuri Pisarevskii<sup>1,2</sup> and Fedor Potemkin<sup>3,\*</sup> 

<sup>1</sup> Federal Scientific Research Center “Crystallography and Photonics”, National Research Center «Kurchatov Institute», Leninskiy Prospect 59, 119333 Moscow, Russia; ontonic@gmail.com (A.K.); fpilyak@yandex.ru (F.P.); ibragimov.eduard-2000@yandex.ru (E.I.)

<sup>2</sup> National Research Center «Kurchatov Institute», Academic Kurchatov Sq. 1, 123182 Moscow, Russia

<sup>3</sup> Faculty of Physics, Lomonosov Moscow State University, 119991 Moscow, Russia

\* Correspondence: mareev.evgeniy@physics.msu.ru (E.M.); potemkin@physics.msu.ru (F.P.)

**Abstract:** The synchronization of laser and X-ray sources is essential for time-resolved measurements in the study of ultrafast processes, including photo-induced piezo-effects, shock wave generation, and phase transitions. On the one hand, optical diagnostics (by synchronization of two laser sources) provides information about changes in vibration frequencies, shock wave dynamics, and linear and nonlinear refractive index behavior. On the other hand, optical pump–X-ray probe diagnostics provide an opportunity to directly reveal lattice dynamics. To integrate two approaches into a unified whole, one needs to create a robust method for the synchronization of two systems with different repetition rates up to the MHz range. In this paper, we propose a universal approach utilizing a field-programmable gate array (FPGA) to achieve precise synchronization between different MHz sources such as various lasers and synchrotron X-ray sources. This synchronization method offers numerous advantages, such as high flexibility, fast response, and low jitter. Experimental results demonstrate the successful synchronization of two different MHz systems with a temporal resolution of 250 ps. This enables ultrafast measurements with a sub-nanosecond resolution, facilitating the uncovering of complex dynamics in ultrafast processes.

**Keywords:** FPGA; synchrotron radiation source; ultrashort lasers; synchronization



**Citation:** Marchenkov, N.; Mareev, E.; Kulikov, A.; Pilyak, F.; Ibragimov, E.; Pisarevskii, Y.; Potemkin, F. Hybrid Approach for Multiscale and Multimodal Time-Resolved Diagnosis of Ultrafast Processes in Materials via Tailored Synchronization of Laser and X-ray Sources at MHz Repetition Rates. *Optics* **2024**, *5*, 1–10. <https://doi.org/10.3390/opt5010001>

Academic Editor: Clare C. Byeon

Received: 18 November 2023

Revised: 24 December 2023

Accepted: 11 January 2024

Published: 16 January 2024



**Copyright:** © 2024 by the authors. Licensee MDPI, Basel, Switzerland. This article is an open access article distributed under the terms and conditions of the Creative Commons Attribution (CC BY) license (<https://creativecommons.org/licenses/by/4.0/>).

## 1. Introduction

The understanding of atomic structure plays a dominant role in scientific research. Significantly, important discoveries concerning structural information have often paved the way for the emergence of new fields. For instance, the observation of X-ray diffraction from crystal lattices laid the groundwork for modern solid-state physics, demonstrating that crystal structures can be obtained through the measurement of X-ray diffraction patterns [1]. However, traditional diffraction methods have primarily provided a static view of the structures. While time-resolved methods have allowed for the measurement of structural changes, directly observing the atomic motions underlying these changes has remained elusive. The timescale for these changes typically falls within the femtosecond range, approximately from  $10^{-12}$  to  $10^{-14}$  s, comparable to the duration of molecular vibrations. Although femtosecond laser pulses have enabled optical measurements with a femtosecond resolution, optical techniques alone cannot offer a direct view of the atomic structure [2,3]. In a typical pump–probe experiment, the pump pulse is used to excite the system, inducing changes in its electronic, vibrational, or structural properties. These changes are monitored by the probe pulse to measure the resultant response [3].

By varying the time delay between the pump and probe pulses, the evolution of the system's dynamics can be captured with ensured temporal resolution [4–6]. Detection of the probe signal can be accomplished using a range of techniques, including photodiodes, streak cameras, transient absorption spectroscopy, or time-resolved spectroscopy [7]. These methods allow for the measurement of various optical properties, such as absorption, reflectivity, transmission, or emission, as a function of the time delay between the pump and probe pulses [8,9].

In optical pump–probe diagnostics, information regarding structural changes has only been indirectly inferred from the secondary effects exerted on optical properties. Therefore, it is necessary to integrate these methods with X-ray time-resolved techniques to obtain comprehensive information about the dynamics of the medium [10,11]. The development of ultrashort X-ray pulses holds great significance as it enables physical experiments that combine femtosecond time resolution with atomic-scale spatial resolution [12,13]. To achieve temporal resolution, it is necessary to synchronize two different sources of laser and/or X-ray radiation [14]. The difficulty of the synchronization procedure strongly depends on the type of the X-ray source. Such sources as X-ray Free Electron Laser are almost naturally synchronized with other lasers with picosecond and sub-picosecond temporal resolutions [12]. However, the maximum achieved time delays are mostly limited by several nanoseconds [15,16]. By synchronizing these sources, researchers can conduct sophisticated time-resolved experiments that capture the dynamics of ultrafast processes on natural atomic and temporal scales. The second commonly applied method of X-ray generation is laser-plasma sources [17,18]. Using high-intensity femtosecond lasers, it becomes possible to generate high-brightness X-ray radiation, which can be used for time-resolved measurements in the pump–probe approach [19]. The time resolution in such a setup is achieved by mechanically moving the delay line [17]. The time resolution is usually about sub-ps, and the maximal obtained information is limited by several nanoseconds. Finally, one of the most important sources is the synchrotron; however, its synchronization with laser sources is highly complex. The synchronization in this case is commonly achieved by phase-locked loop (PLL) systems, which give the opportunity to investigate the dynamics only up to several nanoseconds with a time resolution of tens of picoseconds [20]. To extend the time delays further, up to the microsecond region, the incorporation of electronic time delays becomes necessary.

In this manuscript, we propose a multimodal hybrid approach for all-optical and X-ray time-resolved diagnostics. The key component of the approach is the synchronization system, which utilizes a field-programmable gate array (FPGA) for the synchronization of two different laser sources or an X-ray synchrotron source and a nanosecond laser system. The FPGA-based synchronization method offers several advantages, such as high flexibility and reconfigurability, fast response, low jitter, and the possibility to change the time delay with no limitations or a maximal value. By leveraging these benefits, we aim to address the challenges associated with achieving precise timing control between different laser systems and a synchrotron with a nanosecond laser. The fine temporal resolution offered by the FPGA-based synchronization technique allows for a comprehensive understanding of the intricate dynamics underlying these processes. We employed two different approaches using FPGA-based synchronization systems to investigate the dynamics of crystal lattices excited by intense laser pulses. Firstly, we utilized a pump–probe optical diagnostic technique to observe the formation of micromodifications and shock wave generation induced by laser pulses in silicon (Si). Secondly, we employed an optical pump–X-ray probe technique to retrieve the dynamics of a lithium niobate (LiNbO<sub>3</sub>) lattice irradiated by a nanosecond laser pulse. Both approaches provided the opportunity to observe the dynamics of ultrafast processes with a nanosecond time resolution on sub-millisecond timescales. In the optical pump–probe diagnostics, we used the trigger from a femtosecond laser (pump) to generate a delay for the nanosecond laser source (probe). In the optical pump–X-ray probe diagnostics, we initially decreased the initial RF signal frequency to 5 Hz and only added a time delay to trigger the signal after that. This provides flexibility in manipulating

the period, shift, and duty cycle of the control TTL signals over a wide range of parameters while maintaining robust synchronization to the initial signal. Additionally, there is no limitation on the maximum time delay, allowing for the observation of the complete evolution of the system perturbed by the pump pulse. Both approaches complement each other, which can provide a comprehensive characterization of the process of ultrafast laser pulse interactions with the crystalline lattice

## 2. Materials and Methods

### 2.1. Samples

Samples of lithium niobate (LiNbO<sub>3</sub>) and silicon were chosen as model crystals to test our method. Lithium niobate has pronounced photovoltaic properties [21,22] and is widely used in piezotechnics and in the microelectronics industry in general. Silicon has a low threshold for radiation damage. During laser ablation, phase transitions can occur in it with the formation of new phases with reduced symmetry, which is currently being actively studied by various methods [23,24]. The LiNbO<sub>3</sub> samples were fabricated from monodomain crystals and had the form of plane-parallel rectangular plates with a normal perpendicular to the 001 axis, 0.5 mm thick and with transverse dimensions of 10 mm × 10 mm. The (001) faces were subjected to mechanochemical polishing in order to remove the disturbed layer and achieve a high X-ray optical quality of the surface. As Si samples, Si wafers (111) with a resistivity of 160 Ω·cm were used (Integral, Belarus).

### 2.2. Optical Pump–Probe Diagnostics

In our experiments, we utilized the pump–probe technique, as shown in Figure 1a. The pump laser pulse (100 μJ, 1030 nm, 200 fs) was tightly focused (NA = 0.45) onto the sample surface. The probe pulse was used to measure and analyze the effects induced by the pump pulse (see Figure 1a). To achieve the desired temporal resolution, we implemented an electronic delay circuit using FPGA and analog electronics. The NI CompactRio with Kintex 7 FPGA (Xilinx, San Jose, CA, USA) served as the primary controller for trigger control. At the FPGA level, the trigger from the femtosecond laser system (Avesta TETA 20) could be shifted with a time step of 10 ns, based on the 100 MHz internal clock of the FPGA (see Figure 1b). The FPGA-based application detects the rising front in the GPIO, and then in the time loop (with a 100 MHz clock) counts down the specified delay. The FPGA was programmed via LabVIEW 2013 software. The frequency of the pump pulse could reach up to 4 kHz, but due to the irreversible changes in the sample's boundary, it was set to 100 Hz (see Figure 1b). This ensured that the sample had enough time to recover between each pump–probe cycle. For fine time delays, a custom analog circuit based on DS1124 (Analog Device, Norwood, MA, USA) was utilized, allowing for increments of 250 ps. This circuit added the desired time delay (with a 4 ns and/or 250 ps time step) to the trigger signal, as marked in Figure 1a,b. The jitter, or timing variability, of the electronic circuit was measured to be less than one nanosecond using a 1 GHz oscilloscope. This ensured precise and accurate control over the timing of the trigger pulses, minimizing any unwanted fluctuations or uncertainties in the experimental setup.

As the probe pulse, we utilized laser pulses generated by two different laser systems: Laser Export Tech 527 (wavelength of 527 nm, time duration of 4 ns, and energy up to 100 μJ) and the Quantel Brio (wavelength of 532 nm, time duration of 4 ns, and energy up to 100 mJ). To generate shock waves and observe micromodifications, we tightly focused an infrared femtosecond laser pulse onto the silicon plate surface. The numerical aperture (NA) of the focusing objective was set to 0.45. Simultaneously, an unfocused nanosecond laser pulse was directed to the same point on the sample at an incident angle of 30 degrees. The reflected light from the sample was collected using a microscopic objective with 100× magnification, and the signal was recorded by a CCD camera (MindVision, Shenzhen, China) (see Figure 1a). By varying the time delay between the pump and probe pulses, we were able to observe the formation of micromodifications and the generation of shock waves. After observing these phenomena, we focused the probe beam onto the sample and

replaced the camera with a photodetector (ODA-03B, Avesta, Moscow, Russia). The signal from the photodetector was acquired using a Python (14-bit, 1 GHz) oscilloscope, which was controlled via LAN. All measurements were fully automated using custom software based on LabVIEW 13. This software facilitated the control and synchronization of the laser pulses, acquisition of the reflected signal, and capturing of photographs of the shock waves. The evolution of the reflected signal and photographs of the shock waves were observed over a 15-microsecond timescale with a time step of 1 ns.

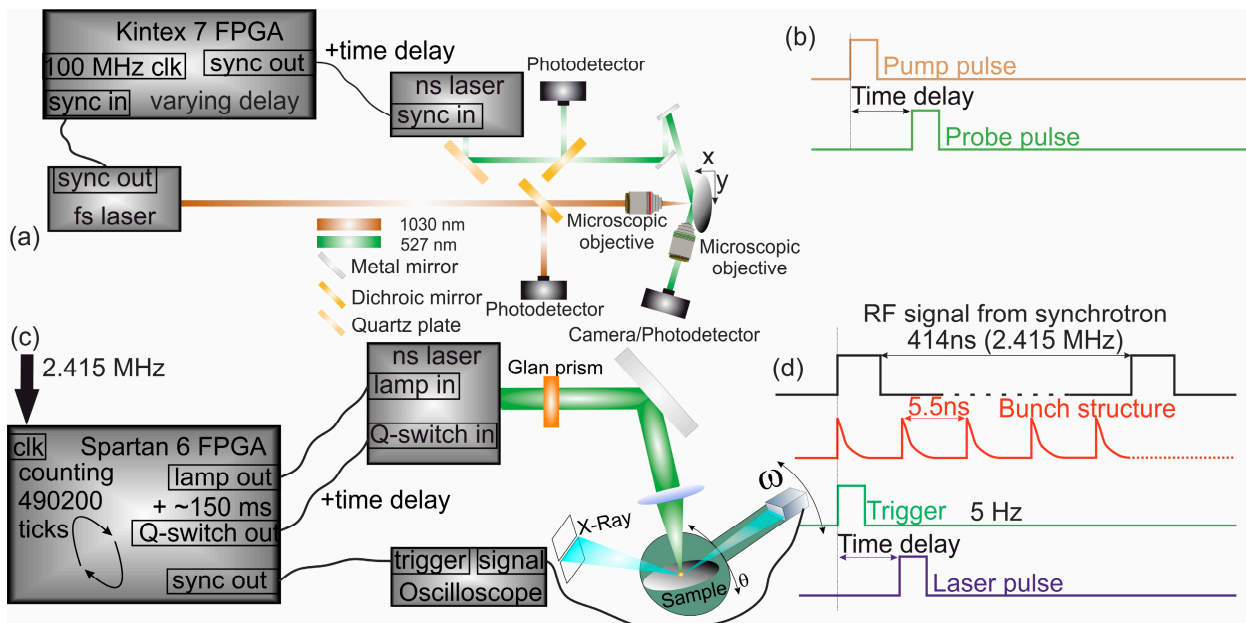


**Figure 1.** (a) Experimental setup of optical pump–optical probe experiment; (b) synchronization scheme of optical pump–optical probe experiment; (c) experimental setup of optical pump–X-ray probe experiment; (d) synchronization scheme of optical pump–X-ray probe experiment.

### 2.3. Optical Pump–X-ray Probe Diagnostics

The X-ray–optical experiments took place at the “RKFM” beamline, dedicated to X-ray crystallography and physical materials science, within the Kurchatov Synchrotron Radiation Source “KISI-Kurchatov”. The successful implementation of synchronization techniques at the “Phase” beamline has expanded the capabilities in experiments at the RKFM beamline [25]. The RKFM beamline gives an opportunity to decrease the diameter of the X-ray beam on the sample up to several micrometers. The beamline design comprises three distinct modules: the X-ray diffraction module (RKFM station), the laser–matter interaction setup, and a synchronization system. All measurements were carried out under ambient room temperature conditions.

#### 2.3.1. X-ray Diffraction Module

Initially, a bending magnet was employed to generate polychromatic synchrotron radiation, which was subsequently collimated using water-cooled slits. The next step involved the monochromatization of the  $\sigma$ -polarized synchrotron radiation. This was achieved by utilizing two horizontally positioned Si single crystals with high structural perfection and symmetric reflections along the (111) plane. These crystals enabled a relative energy divergence of  $2 \cdot 10^{-4}$ . The monochromator was tuned to an energy of 12.000 keV, corresponding to the brightest section of the bending magnet’s spectrum. The resulting beam was further refined through the use of slits with an aperture measuring  $0.5 \times 0.2$  mm.

The characterized beam, which exhibited a temporal structure mirroring the bunch structure of the storage ring, was directed toward a sample placed within an optically

transparent crystal holder. The sample, along with the crystal holder, was mounted on the goniometric system of a Huber multicircle diffractometer (see Figure 1c).

The sample used,  $\text{LiNbO}_3$ , was adjusted to the 0012 X-ray reflection with a precise Bragg angle of  $26.562^\circ$ . This reflection possessed an extinction depth of  $3.7 \mu\text{m}$  and an intrinsic reflectivity half-width of approximately  $2.0 \text{ arcsec}$ . To capture the intensity, a transmission avalanche photodiode detector from FMB Oxford was positioned at the sample's double-Bragg angle. The recorded intensity data were then transmitted to a Python multichannel oscilloscope analyzer (Rudnev-Shilyaev, Moscow, Russia), which offered a sampling rate of 1 GHz and a 14-bit resolution.

### 2.3.2. Laser–Matter Interaction Setup

To initiate the piezo-effect in the  $\text{LiNbO}_3$  sample, a Quantel Brio nanosecond laser was employed. The laser had a maximum pulse energy of 125 mJ, a pulse duration of 4 ns, a repetition rate of 5 Hz, and a focusing spot diameter of  $500 \mu\text{m}$  at an intensity level of  $1/e^2$  and a wavelength of 1064 nm, which further doubled in the nonlinear crystal. Spatial alignment of the laser and X-ray beams was accomplished using a system of mirrors. The laser beam was focused into the sample using a 250 mm focusing lens. Additionally, the laser pulse energy was varied using a Glan prism.

### 2.3.3. Synchronization System

In our experiments, we employed the optical pump–X-ray probe concept, in which the time delay between the laser and X-ray pulses was varied. To achieve synchronization, the laser radiation was synchronized with the rotation period of electron bunches in the SR storage ring. The KISI-Kurchatov synchrotron's storage ring operated in the N-bunches mode, with a total of 75 electron bunches and an orbital period of 414 ns. Each bunch had a duration of approximately 140 ps.

For synchronization, we utilized a home-built system based on a field-programmable gate array (FPGA). The FPGA (Spartan-6, Xilinx) allowed us to create reconfigurable electronic circuits with a low time jitter. In our setup, the high-frequency RF signal generator of the storage ring (operating at 2.415 MHz, with a time jitter better than 1 ps) served as the external clock for the FPGA-based system, ensuring robust synchronization of all signals with the circulating electron bunches. The frequency of the controlling signal was then reduced to 5 Hz by counting down 490,200 ticks of the external trigger in a single process, as illustrated in Figure 2. Signals at a frequency of 5 Hz were used to initiate the lamp and control the electro-optical shutter of the nanosecond laser, with the desired time delays between them (see Figure 1d). The FPGA was programmed using VHDL language via Xilinx ISE 14.7 software. Because we used the synchrotron base RF clock as an FPGA clock, the time jitter was determined by the inner jitter of the FPGA and was about 100 ps.

To achieve time resolution, the analog part of the synchronization system based on DS1124 (Analog Device, USA) adds a controlled delay to the laser trigger signal, with a step of 1 ns. Since the electron bunches on the synchrotron radiation source followed each other with a period of 414 ns, it was necessary to vary the delay within the range of 0–414 ns. The analog signal from the transmission detector was recorded in the time scan of an oscilloscope, with a resolution of 1 ns, synchronized with the laser pulse cycle. The total duration of the time window was  $32.768 \mu\text{s}$ . The synchronization system's operating principle is depicted in Figure 2.

By summing the X-ray diffraction signals for 83 different time delays ( $414 \text{ ns}/5 \text{ ns}$ ), we obtained a comprehensive picture of the temporal changes in the X-ray diffraction signal. The temporal resolution is potentially limited by the duration of the electron bunch, in our case, 140 ps ( $2\sigma$ ). The recorded time signal, on the other hand, is restricted only by the measurement system. In our setup, we used a transmission detector and a Python digital oscilloscope (Rudnev-Shilyaev, Moscow, Russia): 14 bit, 1 GHz. The process of changing the time delay and recording the signal from the detector was fully automated using custom software that controlled the entire registration system via LAN and RS232 connections.

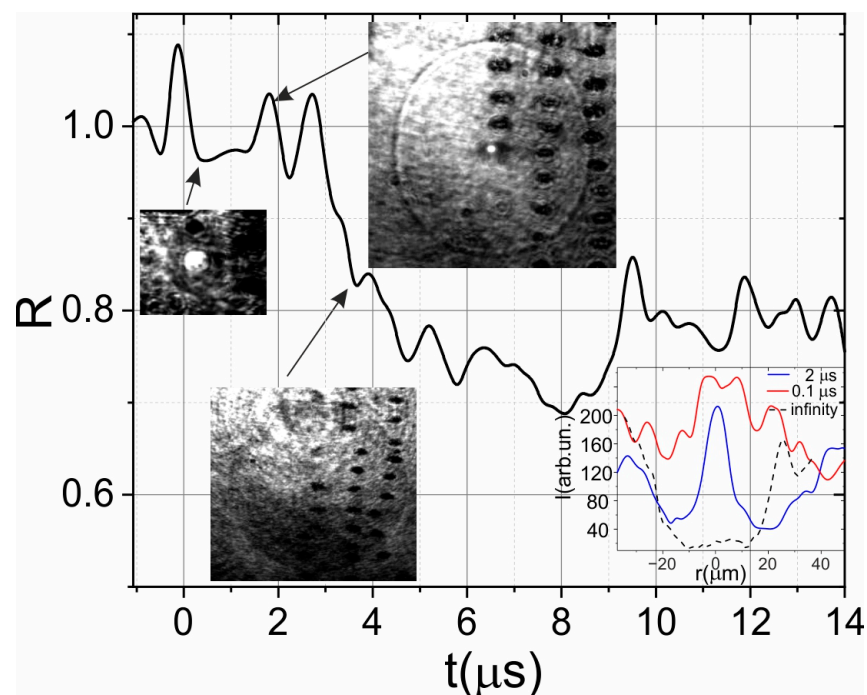


**Figure 2.** Dependence of optical reflection (normalized to the initial value) on the time delay between the pump and probe pulses. The inset provides visual representation of the affected area at specific time delays, where micromodifications are clearly discernible, along with the propagation of a shock wave originating from the impacted region. The white dot observed at the center of the image corresponds to the luminescence emitted by the laser-induced plasma. The bottom inset presents the profile of the affected area at different time delays along a line passing through the center of the micromodification. The peak at the center of the profile corresponds to the presence of laser-induced plasma.

### 2.3.4. Comparison with Other Synchronization Systems

In the context of synchronization systems, the FPGA-based approach does not represent the pinnacle of performance with respect to the minimization of achievable time steps and reduction of jitter, as delineated in Table 1. The most precise synchronization is attained via a phase-locked loop (PLL) mechanism [14]. This method is particularly indispensable when synchronizing synchrotrons with femtosecond lasers, for which it stands as the sole viable option. In the framework of free-electron lasers or laser-plasma X-ray sources, a fraction of the laser pulse energy may be used as a pump pulse, and an optical time delay line can be used [17]. Nonetheless, this technique presents challenges in attaining extended time delays. Conversely, due to the reconfigurability of FPGAs, the maximum time delay is intrinsically unbounded, as it can be programmatically altered by modifying the internal counter. Furthermore, FPGAs offer the flexibility to be configured to a specific laser operation repetition rate, and they present a cost-effective alternative in comparison to other synchronization methods.

**Table 1.** Comparison of different laser-X-ray synchronization systems.

Method	Cost	Scalability	Ease of Implementation	Time Step	Maximal Time Delay	Jitter
PLL	High	High	Hard	<1 ps	Variable	~10–100 fs
FPGA based	Low	High	Easy	~100 ps	Not limited	~100 ps
Analog	Average	Extremely low	Average	~100 ps	Variable	~100 ps
All optical	Variable	Low	Variable	~10 fs	~10 ns	~1 fs

To summarize, using FPGAs for synchronization purposes is beneficial because they can be easily reconfigured for different needs, handle a wide range of time delays, offer good precision at a lower cost, and can be tailored to specific laser repetition rates. This makes FPGAs a versatile and economical choice for various synchronization tasks.

### 3. Results and Discussion

#### 3.1. Optical Diagnostics of Shock Wave Generation and Micromodification Formation

The optical diagnostics could reveal the first stages of the laser ablation of Si. The magnified image of the surface reveals distinct phenomena occurring after laser impact in a timescale of approximately 100 ns. The combination of time-resolved microscopy and time-resolved reflectance provides an opportunity to reveal the evolution of the laser's impact on the material. Prior to the formation of a micromodification, a darkened region emerges, leading to a rapid decrease in reflection. This is indicated by the inset in Figure 2. Subsequently, a shock wave is generated, accompanied by the formation of a micromodification. Initially, the size of the micromodification is larger than its residual size, but the reflection coefficient is higher, as shown by the modification profiles in the inset of Figure 2. The size of the residual micromodification stabilizes at around 1  $\mu\text{s}$ , as evidenced by the transverse profile of the resulting micromodification. Plasma luminescence in the center of the profile appears as a bright dot. Increasing the delay between the pump and probe pulses leads to a decrease in the albedo of the affected area until it reaches saturation. Additionally, the region where the albedo change is observed decreases for longer time delays (see Figure 2). Laser ablation induces high pressures and temperatures, resulting in the generation of a shock wave [26]. The laser-induced shock wave propagates from the impact area at a velocity of approximately 15 km/s, leaving the spatial overlap region between the laser and X-ray beams in approximately 4  $\mu\text{s}$ . Notably, behind the shock wave front, the presence of dark regions, indicating a change in albedo, is observed. The change in the albedo could serve as an indicator of phase transitions.

#### 3.2. X-ray Time-Resolved Diagnostics of the Piezo-Effect in $\text{LiNbO}_3$

Compared to optical pump-probe diagnostics, X-ray time-resolved diagnostics of lattice dynamics induced by laser pulses are more intricate. One of the key challenges is the requirement to measure the X-ray rocking curve for all time delays. This entails obtaining time-resolved dynamics for at least five different diffraction angles. The resulting dynamics can be visualized as a "heat map", with the diffraction angle and time delay as axes (see Figure 3a). This visualization helps to capture the complex temporal evolution of lattice dynamics induced by the laser pulses. The analysis of such heat maps provides valuable insights into the structural and dynamical changes occurring in the material on ultrafast timescales.

We performed the measurement of the X-ray rocking curve for eight angles and during 32 microseconds after laser impact and with a 1-nanosecond time step. From the heat map, we also calculated the evolution of the rocking curve width (at FWHM) and the evolution of the shift of the center of gravity, which was calculated using Equation (1) (see Figure 3).

$$\theta_0 = \frac{\sum_i \theta_i I_i}{\sum_i I_i} \quad (1)$$

where  $\theta_0$  is the center of gravity,  $\theta_i$  is the diffraction angle, and  $I_i$  is the intensity of the X-ray obtained for this angle.

In our experiment, we conducted measurements of the X-ray rocking curve for a total of eight different angles. These measurements were performed over a 32-microsecond time interval after the laser impact, with a time step resolution of 1 nanosecond. By analyzing the obtained data, we constructed a heat map that visualizes the dynamics of the X-ray rocking curve as a function of both diffraction angle and time delay. Additionally, we extracted valuable information from the heat map by calculating the evolution of three key

parameters: the width of the rocking curve at the full width at half maximum (FWHM), the integral intensity of the signal for different angles, and the shift in the center of gravity (Figure 3). The center of gravity shift was determined using Equation (1), which provides a quantitative measure of the displacement of the diffraction peak due to lattice dynamics induced by the laser pulse.

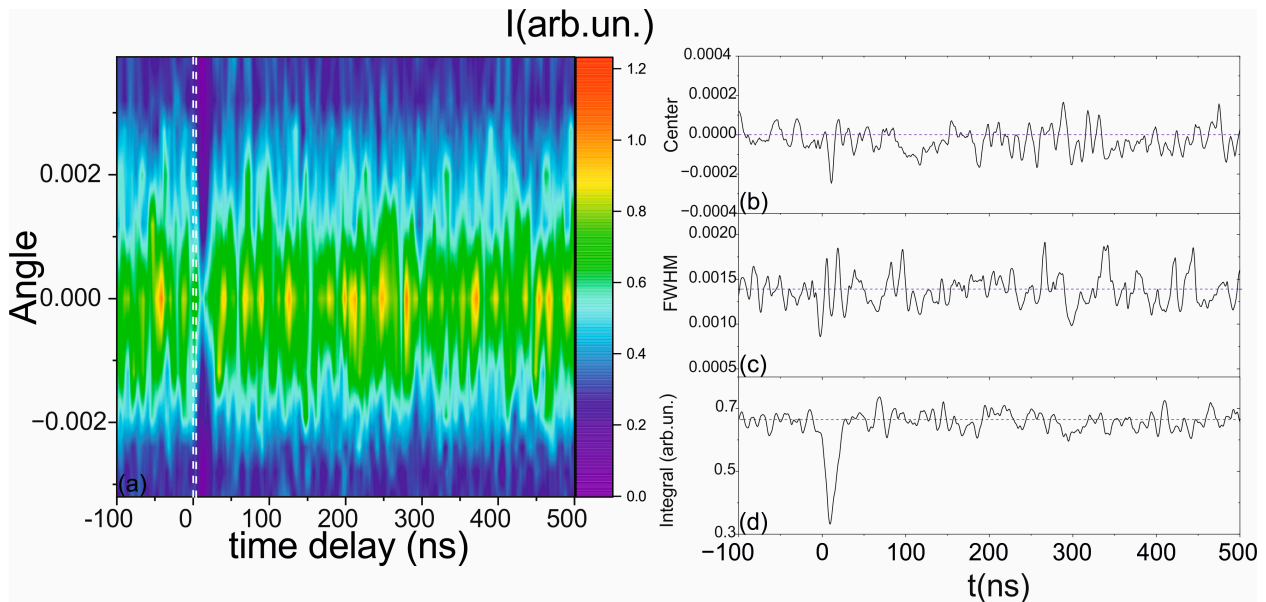


**Figure 3.** Dynamics of X-ray rocking curve after laser impact on the LiNbO<sub>3</sub>. (a) Three-dimensional “heat map”; white dotted lines show the time interval of laser pulse impact, (b) dynamics of center of gravity shift, (c) dynamics of X-ray rocking curve width (FWHM), and (d) dynamics of the integral intensity of the X-ray rocking curve. The blue dotted lines show the initial level in (b–d).

By analyzing the evolution of the rocking curve width and center of gravity shift over time, we gain valuable insights into the structural and dynamical changes occurring in the material following the laser impact. These measurements and calculations provide important information for understanding the behavior of the lattice dynamics and its response to laser-induced excitation. The “heat map” generated from the X-ray rocking curve measurements clearly reveals the moment of laser impact on the sample, marked as white lines in Figure 3. Immediately after the laser impact, there is a noticeable decrease in the integral intensity of the rocking curve. This reduction is attributed to the disorganization of atoms within the material. Additionally, the center of gravity of the rocking curve exhibits slight oscillations during this initial period. The main dynamics of the lattice can be observed over a time interval of approximately 100 ns following the laser impact. This time period is characterized by significant changes in the structural and dynamical properties of the material. These dynamics may include processes such as lattice rearrangement, energy transfer, and relaxation phenomena. The detailed analysis of this 100 ns time interval provides important insights into the behavior of the material under the influence of the laser impulse.

The time-resolved experiments in the synchrotron–laser facility provide an opportunity to investigate lattice dynamics on sub-millisecond timescales with a sub-nanosecond time resolution, which gives an opportunity to investigate comparatively “long” processes such as laser-induced shock wave propagation or piezoelectric deformation, observed as a result of photoinduced electric field formation. The combination with optical methods provides an opportunity for additional diagnostics with such methods as spectroscopy, microscopy, etc.

#### 4. Conclusions

In this study, we employed both optical pump–probe and X-ray time-resolved diagnostics to investigate the lattice dynamics induced by laser pulses on a sample material. Both approaches complement each other and provide the opportunity to observe the dynamics of ultrafast processes with a nanosecond time resolution on sub-millisecond timescales. The optical pump–probe diagnostics allows us to observe the formation of micromodifications and the generation of shock waves following the laser impact. The X-ray time-resolved diagnostic captured the intricate temporal evolution of the material’s structure. We observed a clear moment of laser impact, characterized by a drop in the integral of the rocking curve and slight oscillations in the center of gravity.

Both methods indicate the disordering of atoms and the immediate response of the lattice to the laser pulse. Furthermore, the main dynamics of the lattice were found to occur within a 100 ns time interval after the laser impact. This period exhibited significant changes in the structural and dynamic properties of the material. Processes such as lattice rearrangement, energy transfer, and relaxation phenomena likely contributed to these observed dynamics. The detailed analysis of this time interval allowed us to gain a deeper understanding of the material’s behavior under the influence of the laser pulse. Overall, our findings demonstrate the complementary nature of optical pump–probe and X-ray time-resolved diagnostics in studying the lattice dynamics induced by laser pulses. The optical techniques provided valuable information about the formation of micromodifications and shock waves, while the X-ray methods allowed for a more detailed and complex analysis of the material’s structural changes. Together, these results enhance our understanding of the ultrafast dynamics of materials and have implications for various scientific and technological applications.

**Author Contributions:** Conceptualization, F.P. (Fedor Potemkin) and E.M.; methodology, F.P. (Fedor Potemkin), E.M. and A.K.; software, E.M.; validation, E.I. and F.P. (Fedor Pilyak); formal analysis, N.M.; investigation, all authors; resources, F.P. (Fedor Potemkin), N.M. and Y.P.; data curation, E.M.; writing—original draft preparation, E.M. and F.P. (Fedor Potemkin); writing—review and editing, all authors; visualization, E.M.; supervision, F.P. (Fedor Potemkin); project administration, N.M.; funding acquisition, E.M. and F.P. (Fedor Potemkin). All authors have read and agreed to the published version of the manuscript.

**Funding:** Russian Science Foundation, grant No. 23-73-00039. The time-resolved X-ray optical approach was funded by the framework of the Program of development of Moscow university and the National project “Science and universities”.

**Institutional Review Board Statement:** Not applicable.

**Informed Consent Statement:** Not applicable.

**Data Availability Statement:** The data presented in this study are available on request from the corresponding author. The data are not publicly available due to privacy.

**Conflicts of Interest:** The authors declare no conflicts of interest.

#### References

1. Fetisov, G.V. X-ray Diffraction Methods for Structural Diagnostics of Materials: Progress and Achievements. *Uspekhi Fiz. Nauk* **2020**, *190*, 2–36. [[CrossRef](#)]
2. Sokolowski-Tinten, K.; Von Der Linde, D. Ultrafast phase transitions and lattice dynamics probed using laser-produced X-ray pulses. *J. Phys. Condens. Matter* **2004**, *16*, R1517. [[CrossRef](#)]
3. Mareev, E.; Minaev, N.; Epifanov, E.; Tsymbalov, I.; Sviridov, A.; Gordienko, V. Time-Resolved Optical Probing of the Non-Equilibrium Supercritical State in Molecular Media under Ns Laser-Plasma Impact. *Opt. Express* **2021**, *29*, 33592. [[CrossRef](#)] [[PubMed](#)]
4. Li, R.; Ashour, O.A.; Chen, J.; Elsayed-Ali, H.E.; Rentzepis, P.M. Femtosecond Laser Induced Structural Dynamics and Melting of Cu (111) Single Crystal. An Ultrafast Time-Resolved X-ray Diffraction Study. *J. Appl. Phys.* **2017**, *121*, 055102. [[CrossRef](#)]
5. Pushkin, A.; Migal, E.; Suleimanova, D.; Mareev, E.; Potemkin, F. High-Power Solid-State Near- and Mid-IR Ultrafast Laser Sources for Strong-Field Science. *Photonics* **2022**, *9*, 90. [[CrossRef](#)]

6. Guo, B.; Sun, J.; Lu, Y.F.; Jiang, L. Ultrafast Dynamics Observation during Femtosecond Laser-Material Interaction. *Int. J. Extrem. Manuf.* **2019**, *1*, 032004. [[CrossRef](#)]
7. Noack, J.; Vogel, A. Single-Shot Spatially Resolved Characterization of Laser-Induced Shock Waves in Water. *Appl. Opt.* **1998**, *37*, 4092–4099. [[CrossRef](#)]
8. Lindenberg, A.M.; Larsson, J.; Sokolowski-Tinten, K.; Gaffney, K.J.; Blome, C.; Synnergren, O.; Sheppard, J.; Caleman, C.; MacPhee, A.G.; Weinstein, D.; et al. Atomic-Scale Visualization of Inertial Dynamics. *Science* **2005**, *308*, 392–395. [[CrossRef](#)]
9. Reiter, F.; Graf, U.; Serebryannikov, E.E.; Schweinberger, W.; Fiess, M.; Schultze, M.; Azzeer, A.M.; Kienberger, R.; Krausz, F.; Zheltikov, A.M.; et al. Route to Attosecond Nonlinear Spectroscopy. *Phys. Rev. Lett.* **2010**, *105*, 243902. [[CrossRef](#)] [[PubMed](#)]
10. McBride, E.E.; Krygier, A.; Ehnes, A.; Galtier, E.; Harmand, M.; Konôpková, Z. Phase Transition Lowering in Dynamically-Compressed Silicon. *Nat. Phys.* **2019**, *15*, 89–94. [[CrossRef](#)]
11. Brown, S.B.; Gleason, A.E.; Galtier, E.; Higginbotham, A.; Arnold, B.; Fry, A.; Granados, E.; Hashim, A.; Schroer, C.G.; Schropp, A.; et al. Direct Imaging of Ultrafast Lattice Dynamics. *Sci. Adv.* **2019**, *5*, eaau8044. [[CrossRef](#)]
12. Trigo, M.; Dean, M.P.M.; Reis, D.A. Ultrafast X-ray Probes of Dynamics in Solids. *arXiv* **2021**, arXiv:2108.05456.
13. Siders, C.W.; Cavalleri, A.; Sokolowski-Tinten, K.; Tóth, C.; Guo, T.; Kammler, M.; Horn Von Hoegen, M.; Wilson, K.R.; Von Der Linde, D.; Barty, C.P.J. Detection of Nonthermal Melting by Ultrafast X-ray Diffraction. *Science* **1999**, *286*, 1340–1342. [[CrossRef](#)] [[PubMed](#)]
14. Potemkin, F.V.; Mareev, E.I.; Garmatina, A.A.; Nazarov, M.M.; Fomin, E.A.; Stirin, A.I.; Korchuganov, V.N.; Kvardakov, V.V.; Gordienko, V.M.; Panchenko, V.Y.; et al. Hybrid X-Ray Laser-Plasma/Laser-Synchrotron Facility for Pump-Probe Studies of the Extreme State of Matter at NRC “Kurchatov Institute”. *Rev. Sci. Instrum.* **2021**, *92*, 053101. [[CrossRef](#)] [[PubMed](#)]
15. Schropp, A.; Hoppe, R.; Meier, V.; Patommel, J.; Seiboth, F.; Ping, Y.; Hicks, D.G.; Beckwith, M.A.; Collins, G.W.; Higginbotham, A.; et al. Imaging Shock Waves in Diamond with Both High Temporal and Spatial Resolution at an XFEL. *Sci. Rep.* **2015**, *5*, 11089. [[CrossRef](#)]
16. Inoue, I.; Inubushi, Y.; Sato, T.; Tono, K.; Katayama, T.; Kameshima, T.; Ogawa, K.; Togashi, T.; Owada, S.; Amemiya, Y.; et al. Observation of Femtosecond X-ray Interactions with Matter Using an X-ray-X-ray Pump-Probe Scheme. *Proc. Natl. Acad. Sci. USA* **2016**, *113*, 1492–1497. [[CrossRef](#)]
17. Holtz, M.; Hauf, C.; Hernández Salvador, A.A.; Costard, R.; Woerner, M.; Elsaesser, T. Shift-Current-Induced Strain Waves in LiNbO<sub>3</sub> Mapped by Femtosecond X-Ray Diffraction. *Phys. Rev. B* **2016**, *94*, 104302. [[CrossRef](#)]
18. Weisshaupt, J.; Juvé, V.; Holtz, M.; Ku, S.; Woerner, M.; Elsaesser, T.; Baltuška, A. High-brightness table-top hard X-ray source driven by sub-100-femtosecond mid-infrared pulses. *Nat. Photonics* **2014**, *8*, 927–930. [[CrossRef](#)]
19. Martín, L.; Benlliure, J.; Cortina-Gil, D.; Haruna, A.; Ruiz, C. Validation of a Laser Driven Plasma X-ray Microfocus Source for High Resolution Radiography Imaging. *Phys. Medica* **2021**, *82*, 163–170. [[CrossRef](#)]
20. Banchi, L.; Rossi, F.; Ferianis, M.; Bogoni, A.; Potì, L.; Ghelfi, P. Synchronization of 3GHz Repetition Rate Harmonically Mode-Locked Fiber Laser for Optical Timing Applications. In Proceedings of the 8th European Workshop Beam Diagnostics Instrumentation Particle Accelerator DIPAC 2007, Venezia, Italy, 20–23 May 2007; pp. 358–360.
21. Gerson, R.; Kirchoff, J.F.; Halliburton, L.E.; Bryan, D.A. Photoconductivity Parameters in Lithium Niobate. *J. Appl. Phys.* **1986**, *60*, 3553–3557. [[CrossRef](#)]
22. Gerson, R.; Bryan, A.; Douglas, M.; Louis, S. Bulk Photovoltaic Effect in Commercial Lithium Niobate Crystals. *SPIE* **1983**, *380*, 261–265.
23. Rapp, L.; Haberl, B.; Pickard, C.J.; Bradby, J.E.; Gamaly, E.G.; Williams, J.S.; Rode, A.V. Experimental Evidence of New Tetragonal Polymorphs of Silicon Formed through Ultrafast Laser-Induced Confined Microexplosion. *Nat. Commun.* **2015**, *6*, 7555. [[CrossRef](#)] [[PubMed](#)]
24. Liu, Y.; Ding, Y.; Xie, J.; Xu, L.; Wha Jeong, I.; Yang, L. One-Step Femtosecond Laser Irradiation of Single-Crystal Silicon: Evolution of Micro-Nano Structures and Damage Investigation. *Mater. Des.* **2023**, *225*, 111443. [[CrossRef](#)]
25. Kovalchuk, M.V.; Borisov, M.M.; Garmatina, A.A.; Gordienko, V.M.; Zheltikov, A.M.; Kvardakov, V.V.; Korchuganov, V.N.; Likhachev, I.A.; Mareev, E.I.; Mitrofanov, A.V.; et al. Laser-Synchrotron Facility of the National Research Centre “Kurchatov Institute”. *Crystallogr. Rep.* **2022**, *67*, 717–728. [[CrossRef](#)]
26. Norman, G.E.; Starikov, S.V.; Stegailov, V.V.; Saitov, I.M.; Zhilyaev, P.A. Atomistic Modeling of Warm Dense Matter in the Two-Temperature State. *Contrib. Plasma Phys.* **2013**, *53*, 129–139. [[CrossRef](#)]

**Disclaimer/Publisher’s Note:** The statements, opinions and data contained in all publications are solely those of the individual author(s) and contributor(s) and not of MDPI and/or the editor(s). MDPI and/or the editor(s) disclaim responsibility for any injury to people or property resulting from any ideas, methods, instructions or products referred to in the content.